



University of Tennessee, Knoxville
**TRACE: Tennessee Research and Creative
Exchange**

Chancellor's Honors Program Projects


Supervised Undergraduate Student Research
and Creative Work

5-2012

Physical Adsorption of Gases onto Mesoporous Silica Material SBA-15

Sean C. Forrest
sforres2@utk.edu

Follow this and additional works at: https://trace.tennessee.edu/utk_chanhonoproj

 Part of the [Materials Chemistry Commons](#), and the [Physical Chemistry Commons](#)

Recommended Citation

Forrest, Sean C., "Physical Adsorption of Gases onto Mesoporous Silica Material SBA-15" (2012).
Chancellor's Honors Program Projects.
https://trace.tennessee.edu/utk_chanhonoproj/1567

This Dissertation/Thesis is brought to you for free and open access by the Supervised Undergraduate Student Research and Creative Work at TRACE: Tennessee Research and Creative Exchange. It has been accepted for inclusion in Chancellor's Honors Program Projects by an authorized administrator of TRACE: Tennessee Research and Creative Exchange. For more information, please contact trace@utk.edu.

Physical Adsorption of Gases onto Mesoporous Silica Material SBA-15

Sean Curtis Forrest

May 2012

University of Tennessee, Knoxville

Department of Chemistry

Advisor: Dr. John Z. Larese

1. Background

1.1. *Relevance of Adsorption*

Adsorption is the attachment of particles to a surface through one of several means. The adsorbate is the phase that attaches to the adsorbent; for example, a gas-phase adsorbate molecule may adsorb to the surface of a solid adsorbent. Adsorption plays an important role in many processes including the analytical techniques of gas, high-pressure liquid, and thin-layer chromatography. It can also be used for air purification,¹ the removal of contaminants from aqueous solutions,² and the storage of volatile materials in a less energy-intensive manner than compression.³

1.1.1. *Chemisorption*

Chemical adsorption, called chemisorption, occurs when a molecule or atom is adsorbed to a surface by forming a chemical bond. This process may involve the formation of several bonds in which the adsorbate interacts with multiple atoms or molecules of the adsorbent. Chemisorption can only involve the formation of a single adsorbate-adsorbent bond. Since chemisorption requires the formation of bonds between the adsorbate and the adsorbent, the number of sites at which adsorption can occur is limited. For this reason, chemisorption is limited to monolayer coverage. The enthalpy of chemisorption is often much greater than that of physical adsorption; the distance between the adsorbent and adsorbate is often shorter than for physically-adsorbed molecules.⁴

1.1.2. Physisorption

On the other hand, physical adsorption, or physisorption, occurs when an atom or molecule adsorbs to a surface without the formation of a chemical bond. This interaction is generally the result of a van der Waals interaction between the adsorbate and the adsorbent. Since van der Waals interactions are weaker than chemical bonds, physisorbed molecules are attached to the adsorbent more weakly than chemisorbed molecules. Due to its reliance upon comparatively-weak van der Waals interactions, physical adsorption to a surface is a reversible process. Furthermore, since the number of molecules adsorbed is not limited by the number of sites available for the formation of adsorbate-adsorbent chemical bonds, physical adsorption processes retain the potential for multilayer coverage, which is the formation of several layers of adsorbate molecules on the surface. Additionally, the potential for multilayer coverage leaves open the possibility that adsorbed gas molecules could fill pores in a surface, which would allow for the calculation of pore volume.⁴ Aside from their broad applicability, physisorption studies benefit from the short time required for physisorption equilibria to be reached.⁵

1.2. Adsorption Isotherms

Adsorption isotherms in which small doses of gas are added to an adsorbent while maintaining a constant pressure allow for the characterization of a surface through several means. Since physisorption is a complex process involving various interactions, several models have been developed to aid in the use of experimental

data. Each of these relies upon different assumptions that may affect the model's validity for a given surface.

1.2.1. Langmuir Isotherm

Langmuir developed one of the earliest models of adsorption based on a kinetic approach to explaining a physical adsorption isotherm of a form similar to a typical chemisorption isotherm. This model assumes only a monolayer of adsorbed molecules, a uniform surface, and the absence of interactions among adsorbed molecules.⁴

1.2.2. BET Theory of Adsorption

While the Langmuir isotherm provided an initial model, the Brunauer, Emmett, and Teller (BET) isotherm used a similar kinetic approach that could be applied to multilayer adsorption. BET theory assumes a uniform surface, localized adsorption, no interactions among adsorbed molecules, no limitation on number of adsorbed layers, and that all layers above the first behave like a bulk phase. It also relies upon the assumption that the top layer of adsorbed molecules in a particular location is in dynamic equilibrium with the vapor. Despite these assumptions, BET theory remains useful in the determination of the surface area of an adsorbent.

1.3. Determination of Pore Size

While BET theory and the later Frenkel-Halsey-Hill theory provide a means to calculate the surface area of an adsorbent, other approaches have been developed in order to determine the pore volume and pore radius of porous materials. Since molecules of the adsorbate may be constrained within the pores, the adsorption

interaction may vary depending on the size of the pores. For this reason, different approaches and theories have been developed based on the size of the pore.

1.3.1. Dubinin-Astakhov

The Dubinin-Astakhov theory, which was in itself an extension of Dubinin-Radushkevich theory of adsorption, developed to explain the adsorption of gases in micropores. This theory, which Dubinin called the "theory of volume filling of micropores,"⁶ is a macroscopic thermodynamic approach similar to Polanyi's potential theory of adsorption.⁴ However, it is still used today for the characterization of microporous carbon adsorbents.^{1,2,7} While early studies relied upon the use of benzene as the adsorbate, several approaches have been developed in order to allow for the use of another adsorbate in the Dubinin-Astakhov equation:⁸

$$W = W_0 * \exp \left[- \left(\frac{A}{\beta E_0} \right)^2 \right] \quad [1]$$

where W is the amount adsorbed per mass adsorbent; W_0 is the micropore volume; E_0 is the characteristic energy of adsorption; β is the affinity coefficient; and, A is the change in Gibbs' free energy given by

$$A = RT \ln \frac{P_0}{P} \quad [2]$$

where R is the gas constant; T is temperature; P_0 is the saturated vapor pressure; and P is the pressure of the system.

1.3.2. Kelvin Equation

Adsorption in mesoporous materials such as MCM-41, MCM-48, and SBA-15 differs from either adsorption on a nonporous or microporous surface. The main reason for this difference is pore condensation, which is a phenomenon in which

the gas adsorbed in the pores forms a bulk liquid phase at a pressure less than the saturated vapor pressure of the liquid at that temperature. One of the most common approaches for addressing pore condensation in mesoporous materials is the macroscopic, thermodynamic Kelvin equation:⁴

$$\mu - \mu_0 = -R * T * \ln \frac{p}{p_0} = \frac{-2*\gamma*\cos \theta}{r_m*\Delta\rho} \quad [3]$$

In Equation [3] above, γ is the surface tension of the liquid phase, θ is the contact angle between the liquid phase and the wall of the pore, $\Delta\rho$ is the difference between the orthobaric liquid density and the gas density, and r_m is the “radius of curvature of the meniscus of the pore liquid.”⁴ The mean radius of curvature of the meniscus is the same as the pore radius, or Kelvin radius, for cylindrical pores. The most important aspect of the Kelvin equation is its relation between the chemical potential of a system, $\mu - \mu_0$, to macroscopic quantities.⁴

2. Methods

Over the course of several months, numerous adsorption isotherms were measured using a high-resolution volumetric adsorption isotherm system. In all studies, the adsorbent was SBA-15 made by other members of the research group according to a common literature process. The adsorbates used were methane, ethane, and nitrogen.

2.1. Apparatus

The high resolution volumetric adsorption isotherm system consisted of the various parts in Figure 1. The gas source was either a large bottle or lecture bottle purchased from an industrial supplier at a very high purity and controlled using a flammable regulator. In the case of the nitrogen isotherms used for the surface area calculation, the bleed-off from the liquid nitrogen tank was used as the gas source. The pressure transducer connected to the system allowed for the pressure to be measured accurately and reported to the LabVIEW software using a control box. The sample was loaded into a copper sample cell inside a glovebox containing an argon atmosphere. The sample cell contained a copper spacer to limit the movement of the 0.1-0.15g adsorbent used in this study. The sample cell, which was connected to the gas-handling system using a capillary tube, could be placed on a displacer connected to the helium compressor. The helium compressor cooled the displacer while a temperature controller monitored the temperature of the cell within the evacuated environment of the vacuum jacket. This temperature controller, which was also connected to the computer and LabVIEW software via a control box, could heat the displacer to maintain a constant temperature in the sample cell. Rather than relying upon one pump to evacuate the system, both a rough pump and a turbomolecular

pump were used. This combination of pumps was able to evacuate the system to a baseline pressure of approximately 6×10^{-7} torr. In Figure 1, the small blue circles represent manual valves while the small orange circles represent computer-controlled valves. These computer-controlled valves were important because they allowed for the isotherm to be controlled remotely using a computer program.

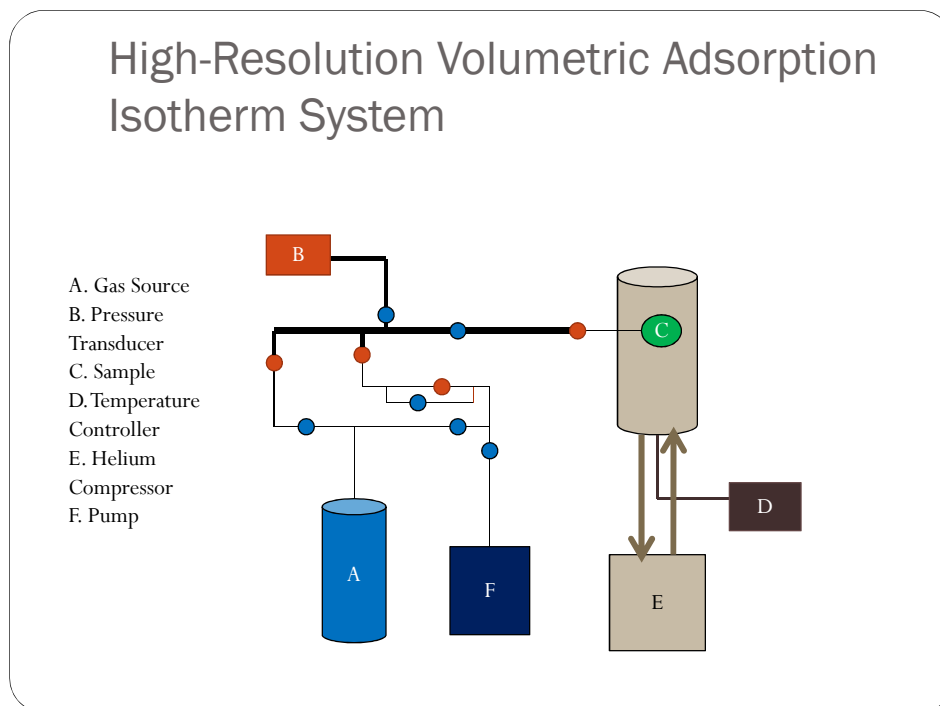


FIGURE 1: Schematic of High-Resolution Volumetric Adsorption Isotherm Station

2.2. Adsorbent

In all of these studies, the adsorbent was SBA-15, which is a mesoporous silica material. The surface area of the material is high, 400-900 m²/g. Figure 2, which is a TEM micrograph from Michael Felty, demonstrates the hexagonal shape of the pores found in SBA-15. In the image, the exceptionally dark portions are gold nanowires. According to Zhou, the material is characterized by a narrow pore size distribution.⁹ The pore size of SBA-15 can be varied between 5 nm and 15 nm.^{10,11} Despite the narrow pore size distribution, SBA-15 has micropores that connect with the mesopores. The temperature and time of the synthesis affect the surface area as well as the number and volume of the micropores.¹²

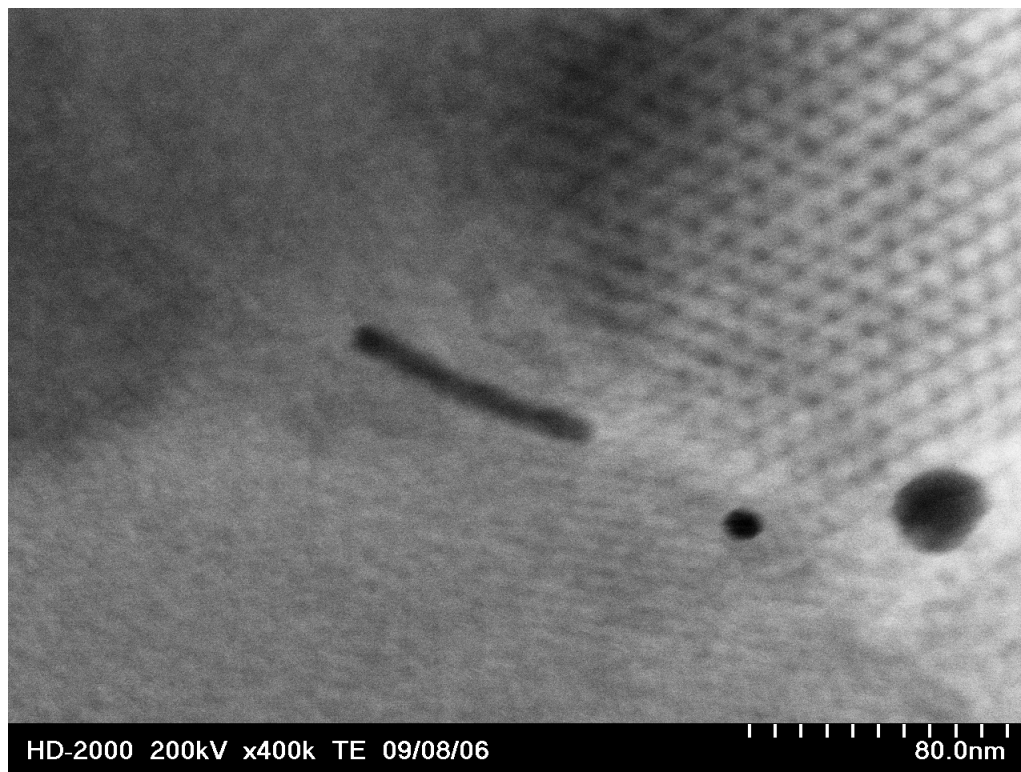


FIGURE 2: TEM Micrograph of SBA-15 with Gold Nanowire

2.3. Adsorbates

In this study, several different adsorbates were used to characterize the surface of the SBA-15 material as well as the adsorbate-adsorbent interactions. In all cases, nonpolar adsorbates were used. Methane was chosen for its spherical symmetry and as a reference for any future studies using longer-chain alkanes. Ethane was chosen in order to determine if the difference in molecular size between it and methane would significantly affect the adsorbate-adsorbent interactions. Since methane and ethane are both nonpolar hydrocarbons, differences in polarity or dipole were not expected to affect the result. Nitrogen was selected because it is the gas most often used for surface area and pore size determinations. Furthermore, it shares some symmetry elements with ethane. For a summary of various properties of these gases, please see Table 1.

Parameter	Methane	Ethane	Nitrogen	
Molecular Weight (g mol^{-1})	16.043	30.069	28.013	
Liquid Density (g cm^{-3})	0.423	0.545	0.808	
Density at STP (g cm^{-3})	0.000717	0.00126	0.00125	
Refractive Index	1.004	1.005	1.199	
Molar Polarizability ⁱ	0.0101	0.173	4.41	
Antoine Equation Coefficients	A ¹³	3.9895	4.50706	3.7362
	B ¹³	443.028	791.3	264.651
	C ¹³	-0.49	-6.422	-6.788

TABLE 1: Properties of Adsorbates Used^{13,14}

ⁱ These values were calculated using equation [17].

For these studies, it was expected that the difference in molecular size would affect the enthalpy and entropy of adsorption for subsequent adsorption steps. In the case of methane, a smaller difference in these thermodynamic quantities was expected because the small molecule should readily access both mesopores and micropores. In the case of ethane, a larger energetic difference was expected because the larger molecule was expected to preferentially fill the larger pores at lower relative pressures.

3. Quantities from Adsorption Isotherm

3.1. Moles Adsorbed

In order to use the adsorption data recorded, the number of moles of gas adsorbed was calculated for each data point in the adsorption isotherm. The initial pressure, final pressure, and sum of the change in pressure were recorded by the LabVIEW program. The initial pressure was that present in the known volume of the gas-handling system at room temperature, which was determined using a series of helium expansions. The initial number of moles was then calculated using the ideal gas law:

$$n_i = \frac{P_i V_i}{RT_i} \quad [4]$$

where P_i is the initial pressure recorded in the LabVIEW software as measured by the pressure transducer, V_i is the initial volume in the gas-handling system, and T_i is the temperature of the room. After gas was introduced into the sample-cell, the system was allowed to reach equilibrium, and the final pressure was recorded. Using the law of conservation of mass, the number of moles in each part of the apparatus could be determined:

$$n_f = n_{known\ volume} + n_{dead\ space} + n_{adsorbed} \quad [5]$$

where $n_{known\ volume}$ is the number of moles in the gas phase in the known volume, $n_{dead\ space}$ is the number of moles in the gas phase in the sample cell, and $n_{adsorbed}$ is the number of moles adsorbed to the surface of the adsorbent.

The ideal gas law relationship was then used to derive an equation for the number of moles of gas adsorbed:

$$n_{adsorbed} = \frac{\sum \Delta P * V_{known}}{RT_{room}} - \frac{P_f V_{dead\ space}}{RT_{sample}} \quad [6]$$

Using Equation 1 above, the number of moles of gas adsorbed was calculated for each data point recorded by the computer program controlling the high-resolution adsorption isotherm station. The term V_{known} is the initial volume into which the gas is dosed from the high-resolution adsorption isotherm system. The term $V_{dead\ space}$, or the dead space volume, is the free volume in the sample cell, which was determined using helium expansions and the ideal gas law. Since this volume, $V_{dead\ space}$, was at the same temperature as the sample, the sample temperature was used to determine the number of moles in the gas phase in the dead space volume.

3.2. Temperature within Sample Cell

Although one calibrated resistance thermometer was used by the temperature controller to monitor the temperature of the sample cell while another recorded the temperature, the temperature inside the sample cell was determined using the Antoine equation:¹⁵

$$\log_{10}(P) = A - \frac{B}{T+C} \quad [7]$$

where P is the saturated vapor pressure of the gas; T is the temperature; and, A , B , and C are the Antoine parameters of the gas. The saturated vapor pressure, which is P_0 , in most subsequent equations, was taken from the LabView Data File as the maximum final pressure. Solving the Antoine equation for temperature gives a more useful form of the equation for the purposes of adsorption studies:

$$T_{trs} = \frac{-B}{\log_{10}(P)-A} - C \quad [8]$$

3.3. Volume of Molecules Adsorbed

In order to create a pore size distribution plot of $\frac{dV_{adsorbed}}{dr}$ versus the Kelvin radius, it is necessary to determine the volume of molecules adsorbed. Since volume

and temperature are directly proportional in the ideal gas law, using the equivalent volume of molecules adsorbed at standard temperature and pressure helps to normalize the values:

$$v_{adsorbed} = \frac{n_{adsorbed} * R * T_0}{P} \quad [9]$$

In this equation, R is the gas constant, T_0 is 273.15 K, and P is 100 kPa.

3.4. BET Surface Area

In order to determine the monolayer coverage and the surface area of an adsorbent, the Brunauer, Emmett, and Teller (BET) theory is often used to model physical adsorption.⁴ Then, the monolayer coverage of a system can be determined by plotting $\frac{x}{n(1-x)}$ versus x :

$$\frac{x}{n*(1-x)} = \frac{1}{c*n_m} + \frac{(c-1)*x}{c*n_m} \quad [10]$$

In this plot, x is the reduced pressure—the final pressure as a fraction of the saturated vapor pressure of the system at a given temperature. The term n is the number of moles of gas adsorbed.

The term c is the BET constant calculated using the parameters of a linear least-squares regression of the BET plot between reduced pressures of 0.05 and 0.30:

$$c = \frac{m}{b} + 1 \quad [11]$$

In this equation, m is the slope of the linear fit of the BET plot while b is the y-intercept of the same regression. These values were also used to determine the number of moles of gas in the adsorbed monolayer, n_m :

$$n_m = \frac{1}{b*c} \quad [12]$$

In this equation, b is the y-intercept of the linear least squares regression of the BET plot, and c is a dimensionless constant.

Then, using the number of moles of gas in the adsorbed monolayer and the average molecular cross-sectional area of the adsorbate, the surface area of the monolayer, A_m , was calculated:

$$A_m = N_0 * n_m * \sigma \quad [13]$$

In this equation, N_0 is Avogadro's number, and σ is the molecular cross-sectional area of the adsorbate on the adsorbent. Since the molecular cross-sectional area is dependent upon the adsorbate-adsorbent interactions and the orientation in which the adsorption occurs, literature values were used to determine this value.^{16,17}

3.5. Two-Dimensional Compressibility

The two-dimensional compressibility, which reflects the response of adsorbed molecules to the spreading pressure, can be used to determine the location at which phase transitions in the film of adsorbed gas occur:¹⁸

$$K_{2D} = \frac{A * p}{k_B * T * n^2 * N_A} * \frac{dn}{dp} \quad [14]$$

In Equation [14] above, A is the surface area, p is the final pressure, T is the temperature, and n is the number of molecules adsorbed. By plotting K_{2D} as a function of chemical potential, μ , the locations of the peaks may be used to determine the temperature at which a phase change occurs.

$$\mu - \mu_0 = -R * T * \ln \frac{p}{p_0} \quad [15]$$

In Equation [15] above, R is the gas constant, T is the temperature, and $\frac{p}{p_0}$ is the reduced pressure. From this relation, it is apparent that the chemical potential of a system is a function of the reduced pressure and temperature.

3.6. Phase Transition

Larher and Angerand demonstrated that tracking the two-dimensional compressibility of a system as a function of chemical potential (temperature) can be useful in determining the temperature at which phase transitions occur.¹⁹ The most important parameter in characterizing this shift is the width of the peak in two-dimensional compressibility reflected by the full-width, half-maximum of the peak.¹⁸ The use of FWHM to represent peak width is especially useful in noisy or irregular peaks; however, some poorly resolved peaks create situations in which difficult decisions regarding data analysis must be made.

3.7. Dubinin-Astakhov Pore Size Distribution

As demonstrated above, Dubinin-Astakhov theory is useful for the determination of the pore size distribution of the micropores in carbon-based materials. However, this theory was extended to adsorption onto mesoporous silica material SBA-15 in order to assess the validity of Dubinin-Astakhov assumptions to a system involving a polar adsorbent containing both micro- and mesopores.

3.7.1. Micropore Volume

In order to use Dubinin-Astakhov theory to create a pore size distribution, a logarithmic form of the Dubinin-Astakhov equation was used:²⁰

$$\log(V) = \log(V_0) - \left[\frac{RT}{\beta E_0} \right]^N * \left[\log \frac{P_0}{P} \right]^N \quad [16]$$

In this equation, V is the volume of gas adsorbed at standard temperature and pressure, V_0 is the micropore capacity, P is the final pressure of the system, and P_0 is the saturated vapor pressure of the gas at temperature T . As usual, R is the gas constant, used in $\text{kJ K}^{-1}\text{mol}^{-1}$. The final two parameters-- N and β --are the

Astakhov exponent and affinity coefficient of the analysis gas. In Dubinin-Radushkevich theory, the exponent was set to a value of 2; however, the Astakhov exponent can be varied across a range of values.ⁱⁱ Wood demonstrated the usefulness of using the ratio of molar polarizabilities (rather than liquid molar volume or parachor) with respect to benzene as a means of determining the affinity coefficient of a gas on an adsorbent not previously studied.⁸ Molar polarizability is a function of several easily-found parameters:

$$P_e = \left(\frac{M_w}{d_L}\right) * \left(\frac{n_D^2-1}{n_D^2+2}\right) \quad [17]$$

In this equation, P_e is the molecular polarizability, M_w is the molecular weight of the gas, d_L is the liquid density, and n_D is the refractive index.

Plotting the logarithm of volume of gas adsorbed, $\log(V)$, as a function of the logarithm of the inverse of reduced pressure, $\log(P_0/P)^N$, allows a linear regression to be used to determine unknown values. The monolayer capacity in equation [16] was determined directly from the y-intercept of the regression:

$$V_0 = 10^{y\text{-intercept}} \quad [18]$$

The characteristic energy, E_0 , was also calculated using the terms of this linear regression:

$$E_0^N = \frac{-(RT)^N}{\beta^{N*m}} \quad [19]$$

In this equation, R is the gas constant; T is temperature; β is the affinity coefficient; and, m is the slope of the linear regression. N is the Astakhov exponent, which was set to 1 in this experiment.

ⁱⁱ Most commercial surface area apparatuses vary this number automatically to minimize the standard error in the y-intercept. In this study, a value of 1 was found to give the lowest standard error in y-intercept and was used for all subsequent calculations.

More important, however, was the calculation of the micropore volume for each data point:

$$W_i = V_i * \frac{\delta_{liquid}}{\delta_{gas,STP}} \quad [20]$$

This value, along with the subsequent equivalent pore diameter calculation, was used to create a pore-size distribution for the SBA-15 sample.

3.7.2. Equivalent Pore Diameter

The equivalent pore diameter was calculated as a function of several values derived from the Dubinin-Astakhov plot:²⁰

$$D = 2 * \left[\frac{-\left(\frac{10^3 \text{ nm}^3/\text{\AA}^3}{\beta E_0}\right)^N}{\ln W_i - \ln W_0} \right]^{1/3N} \quad [21]$$

In equation [21], the value of W_i is the micropore volume calculated using Equation [20] while W_0 is the limiting micropore volume calculated by substituting V_0 for V_i in equation [20]. From this equivalent pore diameter, the equivalent pore radius was calculated:

$$r_{pore} = \frac{D_{pore}}{2} \quad [22]$$

To create a pore-size distribution, the derivative of the micropore volume with respect to equivalent pore radius was plotted against the equivalent pore radius.

3.8. Kelvin Equation Pore Size Distribution

In order to compare the results of the Dubinin-Astakhov equation to those of a more-recognized theory applied to mesoporous materials, the Kelvin equation was used.

3.8.1. Kelvin Radius

The data from an adsorption isotherm can also prove useful for determining the pore size of a mesoporous material such as SBA-15. Macroscopic, thermodynamic approaches to determining pore size can be used if the pores of the adsorbent are of uniform size and shape. The simplest approach relies upon the Kelvin equation:²

$$\mu - \mu_0 = -R * T * \ln \frac{p}{p_0} = \frac{-2*\gamma*\cos\theta}{r_m*\Delta\rho} \quad [23]$$

In Equation [23] above, γ is the surface tension of the liquid phase, θ is the contact angle between the liquid phase and the wall of the pore, $\Delta\rho$ is the difference between the orthobaric liquid density and the gas density, and r_m is the “radius of curvature of the meniscus of the pore liquid.”⁴ The mean radius of curvature of the meniscus is the same as the pore radius, or Kelvin radius, for cylindrical pores. In the case of complete wetting, θ is assumed to be zero. This, along with the common assumption that the orthobaric liquid density is very much greater than the gas density, results in a simplified Kelvin equation:

$$\ln \frac{p}{p_0} = \frac{2*\gamma*\bar{V}}{r_m*R*T} \quad [24]$$

In Equation [24] above, γ is the surface tension of the bulk phase, and \bar{V} is the average molar volume of the liquid phase.²

In order to correct for any interactions between the liquid phase and the wall or the layers of adsorbed molecules, the modified Kelvin equation is used:

$$\ln \frac{p}{p_0} = \frac{-2*\gamma*\cos\theta}{R*T*\Delta\rho*(r_m-t_c)} \quad [25]$$

In Equation [25] above, the new term, t_c , is the statistical thickness before condensation.²

A plot of the derivative of the equivalent volume of gas adsorbed at standard temperature and pressure with respect to pore radius versus the pore radius illustrates the distribution of pore sizes calculated.

3.9. Clausius-Clapeyron

The data from an adsorption can also be used to calculate the thermodynamic quantities associated with a specific adsorption step using the Clausius-Clapeyron equation:⁴

$$\log \frac{p}{p_0} = \frac{-\Delta_{trs}H}{RT} \quad [26]$$

In order to use Equation [26] above, a plot of the logarithm of pressure versus inverse temperature was created, which gives a linear plot:³

$$\log p_f = B^n + \frac{A^n}{T} \quad [27]$$

In Equation [27] above, B^n and A^n are coefficients for a particular adsorption step. The value of p_f used in this equation was the maximum of the first derivative of the standard adsorption isotherm. Using the slope and intercept for the linear trend lines of the plot described in Equation [27], the coefficients B^n and A^n may be determined. From these values, the enthalpy and entropy for the adsorption process of the given layer could be determined:

$$\Delta H^n = -R * (A^n - A^\infty) \quad [28.a]$$

$$\Delta S^n = -R * (B^n - B^\infty) \quad [28.b]$$

The heat of adsorption can also be determined using the coefficients of Clausius-Clapeyron plot:

$$Q_{trs} = R * A^n \quad [28.c]$$

4. Results

4.1. Moles Adsorbed

Figure 3 is a set of adsorption isotherms for methane over the temperature range of 68.82 K to 89.20 K. Two adsorption-desorption isotherms that had crossed others at a reduced pressure of approximately 0.6-0.7 were discarded; this difference was likely a result of a change in temperature or a difference between the standard adsorption program and that used for adsorption-desorption isotherms. The deviation of the 89.20 K isotherm from the others beginning at a reduced pressure of approximately 0.15 was likely caused by temperature fluctuations. At the time, the secondary resistance thermometer was not recorded by the LabVIEW software--an issue that was corrected in subsequent isotherm experiments. From this plot, it becomes apparent that the reduced pressure at which the second layering step is complete decreases with temperature.

Figure 5 is a set of adsorption isotherms for ethane over the temperature range of 114.15 K to 143.25 K. Despite having a larger temperature range and greater number of isotherms than set of methane isotherms, those of ethane generally conform to the expected shape with significant separation among the temperatures only occurring in the riser region, which will be shown to correspond to the completion of the second adsorption step. Unlike the adsorption isotherms for methane, the reduced pressure at which the second layering step is complete increases with temperature.

Figures 4 and 6 are adsorption-desorption isotherms for methane and ethane, respectively, on SBA-15. Both exhibit a significant hysteresis loop, which reflects that the adsorption and desorption processes occur in different manners. As noted in

Lowell, adsorbents with a network of pores such as SBA-15 often exhibit hysteresis due to capillary condensation.⁴

Figure 7 is a set of nitrogen adsorption isotherms from 65.63 K to 80.42 K. These isotherms were performed on a different sample of SBA-15 manufactured using the same process. Unlike both methane and ethane, these isotherms do not appear to complete the adsorption steps at the same relative pressure nor do they approach a maximum number of moles adsorbed. For these reasons, the nitrogen isotherms were not used in any subsequent calculations other than the determination of the BET surface area using one of the sets of data which had the shape expected for nitrogen adsorption onto SBA-15.¹²

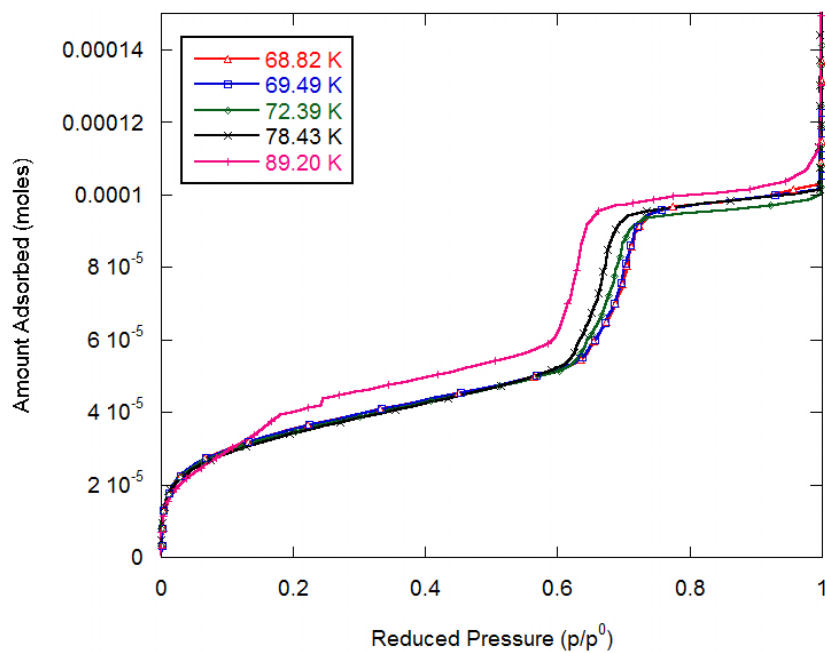


FIGURE 3: Adsorption Isotherms for Methane on SBA-15

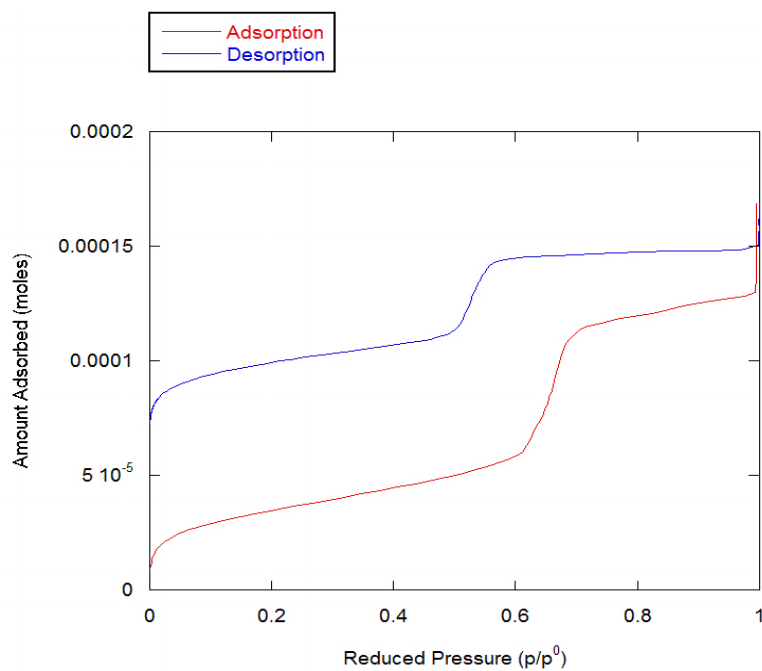


FIGURE 4: Adsorption-Desorption Isotherm for Methane on SBA-15 (78.42 K)

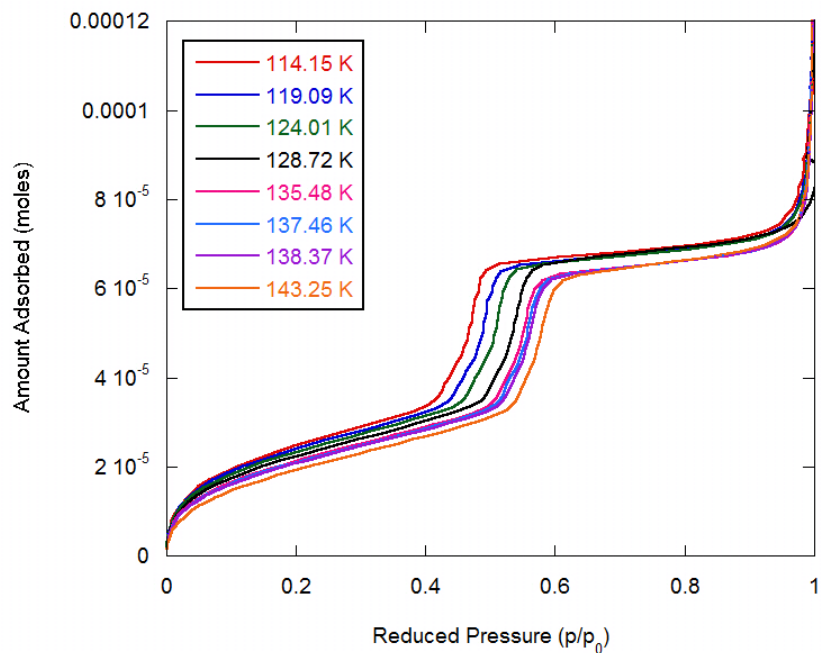


FIGURE 5: Adsorption Isotherms for Ethane on SBA-15

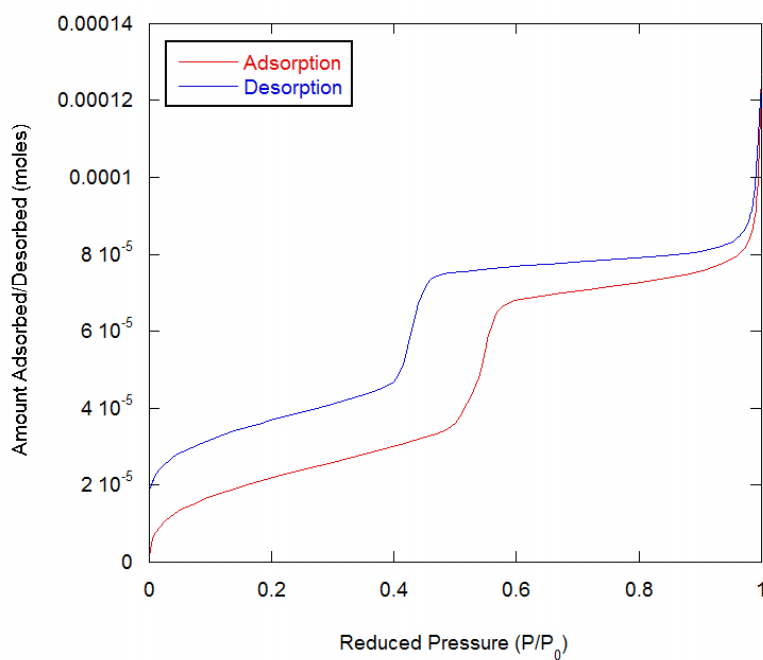


FIGURE 6: Adsorption-Desorption Isotherm for Ethane on SBA-15 (133.75 K)

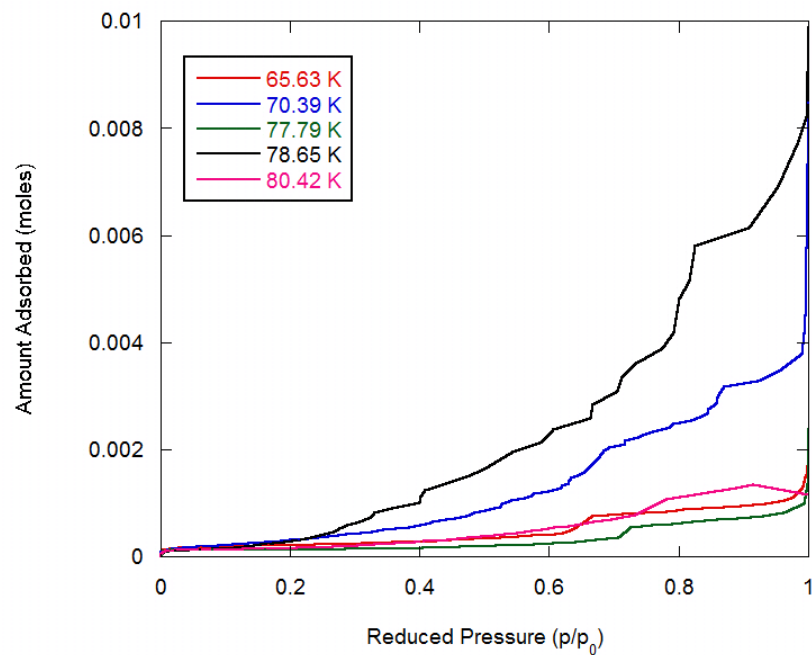


FIGURE 7: Adsorption Isotherms of Nitrogen on SBA-15

4.2. BET Surface Area

Figures 8 and 10 represent plots of an adsorption isotherm and first derivative of the isotherm curve for methane and ethane, respectively, on SBA-15. The maxima in first derivative correspond to the completion of a given adsorption layer. For both of these plots, the completion of the monolayer occurred at a reduced pressure too small to determine accurately without using a very-high resolution isotherm. However, the completion of the second layer occurred at a reduced pressure of approximately 0.65 for methane and 0.50 for ethane.

Figures 9 and 11 represent BET plots for methane and ethane on SBA-15 respectively. By fitting a linear trend line to these plots between reduced pressures of 0.05 and 0.30 and using Equations [10-12], the number of moles in the monolayer could be determined. These values may be found in Table 2. The number of moles of gas adsorbed in the monolayer was greater for methane than for ethane, which is to be expected due to the difference in size of the two gases.

Figure 12 is a plot of an adsorption isotherm for nitrogen on SBA-15 and its first derivative. This isotherm suggests the completion of several different adsorption steps approaching a relative pressure of unity; however, the relatively large step size chosen for the nitrogen isotherms limited the number of data points between which the derivative could be taken. This may have contributed to the numerous local maxima in the first derivative curve for the nitrogen adsorption isotherm.

Figure 13 is a representative BET plot of nitrogen on SBA-15. As with methane and ethane, the number of adsorbed molecules in the monolayer was calculated using Equations [10-12].

Then, using Equation [13] and the average molecular cross-sectional area, the surface area per gram of the SBA-15 sample was determined. In Table 2, several different molecular cross-sectional areas were used for each adsorbate; this reflects the various possible orientations at which adsorption can occur and the nature of the adsorbate-adsorbent interactions. If this interaction is stronger such that the molecules become more closely packed, the average molecular cross-sectional area of the adsorbed molecule decreases. Similarly, if the gas-phase molecule adsorbs in along a different symmetry element, the molecular cross-sectional area may vary. From the data in Table 2, methane and ethane suggest a surface area between $25 \text{ m}^2/\text{g}$ and $30 \text{ m}^2/\text{g}$. The surface area determined using nitrogen adsorption was roughly one order of magnitude greater at between $185 \text{ m}^2/\text{g}$ and $235 \text{ m}^2/\text{g}$. Although neither of these results corresponds with the projected surface area of $400\text{-}900 \text{ m}^2/\text{g}$, the values derived from the BET plot of nitrogen adsorption are on the correct order of magnitude. Had a nitrogen isotherm with higher resolution and at a temperature of 77K been used, the result of this surface area determination may have coincided with the expected range more closely.

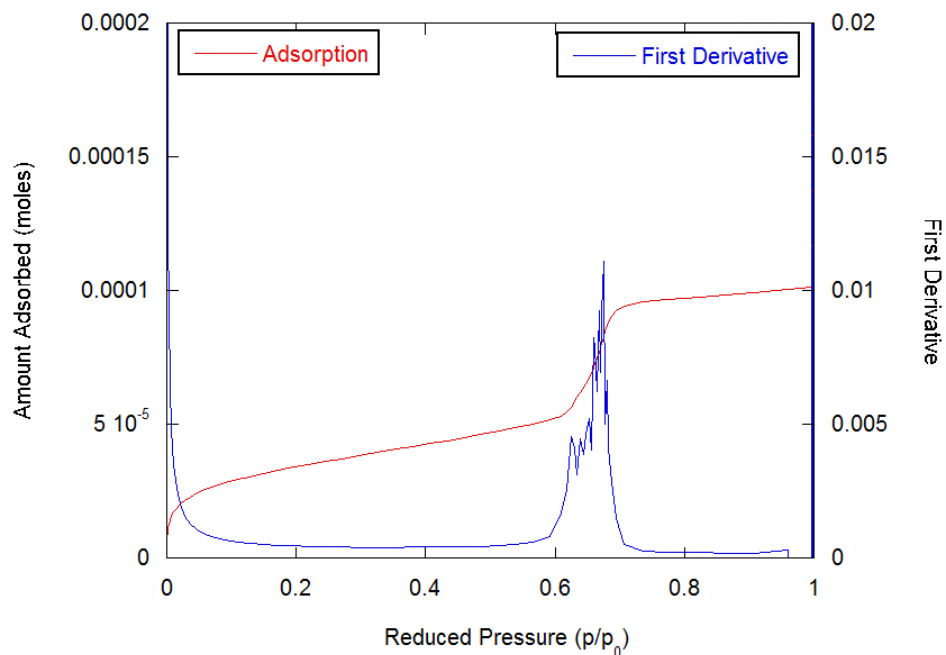


FIGURE 8: Plot of Adsorption Isotherm and First Derivative for Methane on SBA-15 (77.69 K)

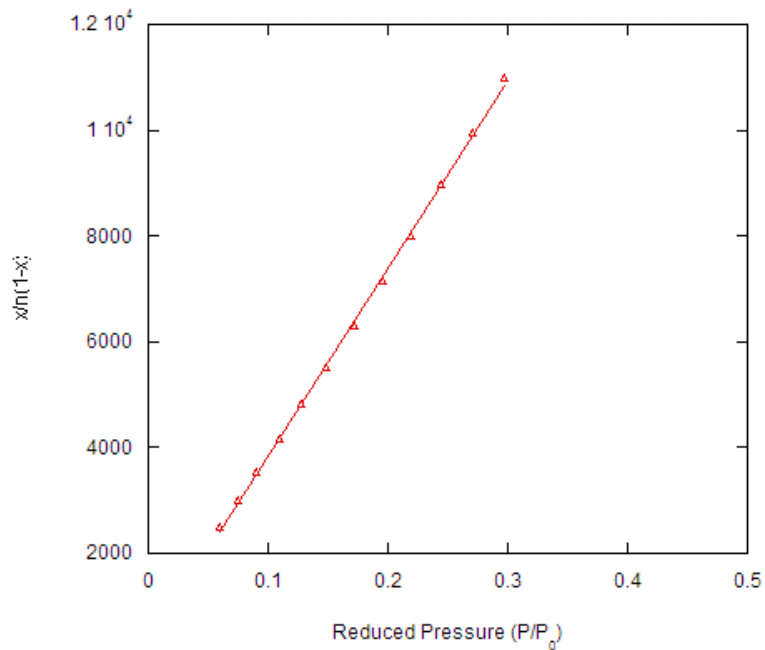


FIGURE 9: Representative BET Plot for Methane on SBA-15 (77.69 K)

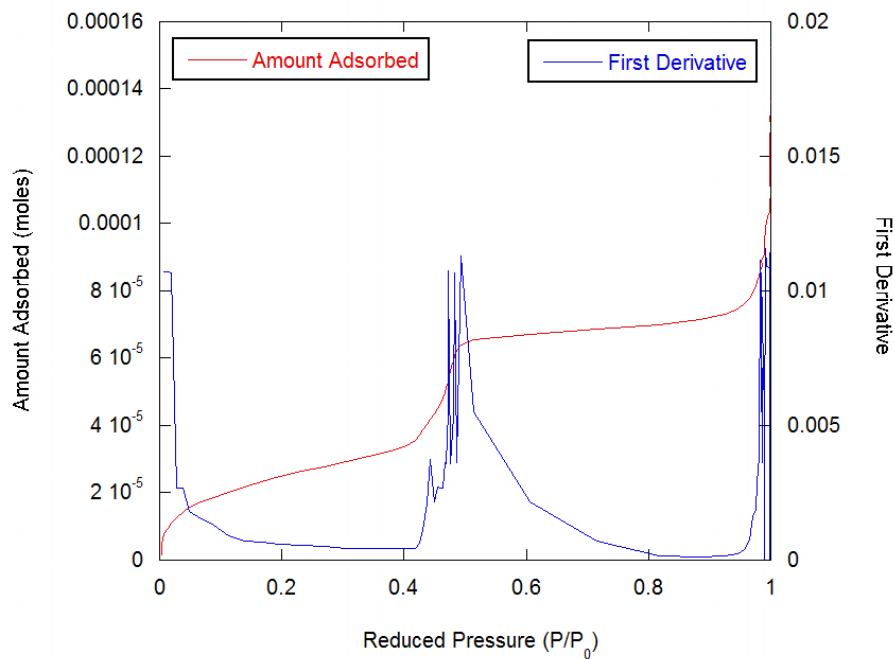


FIGURE 10: Plot of Adsorption Isotherm and First Derivative for Ethane on SBA-15 (114.15 K)

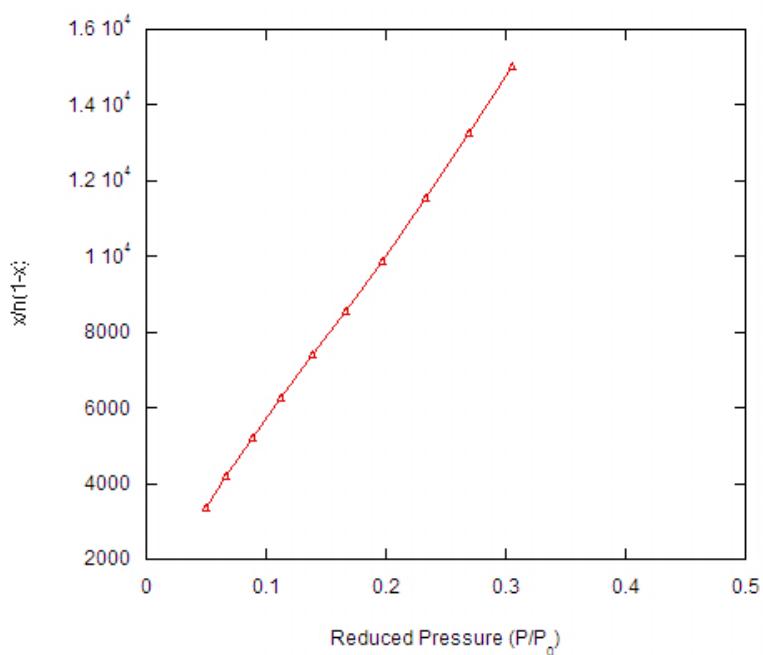


FIGURE 11: Representative BET Plot for Ethane on SBA-15 (114.15 K)

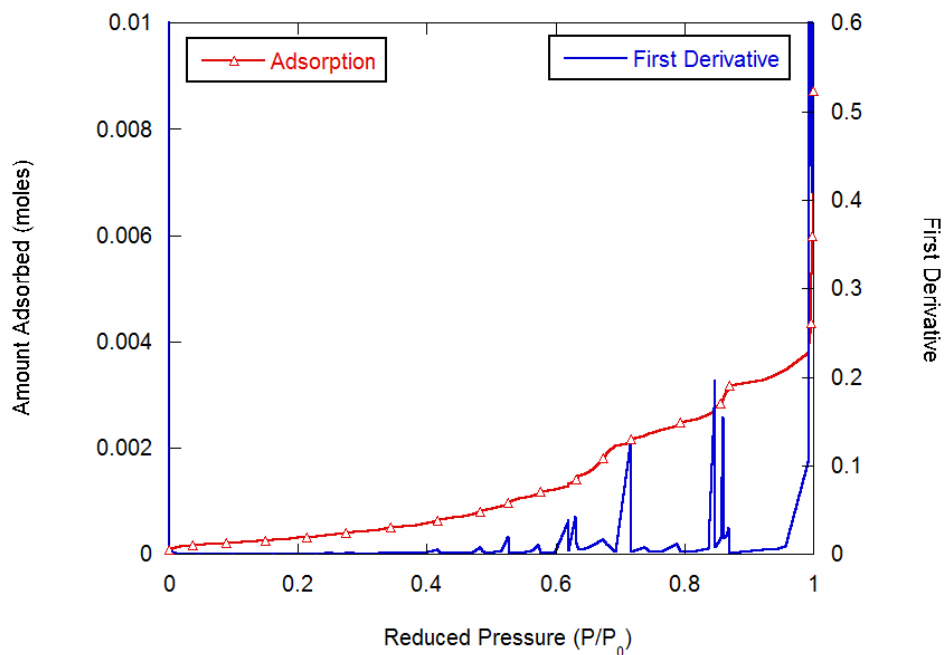


FIGURE 12: Plot of Adsorption Isotherm and First Derivative for Nitrogen on SBA-15 (70.39 K)

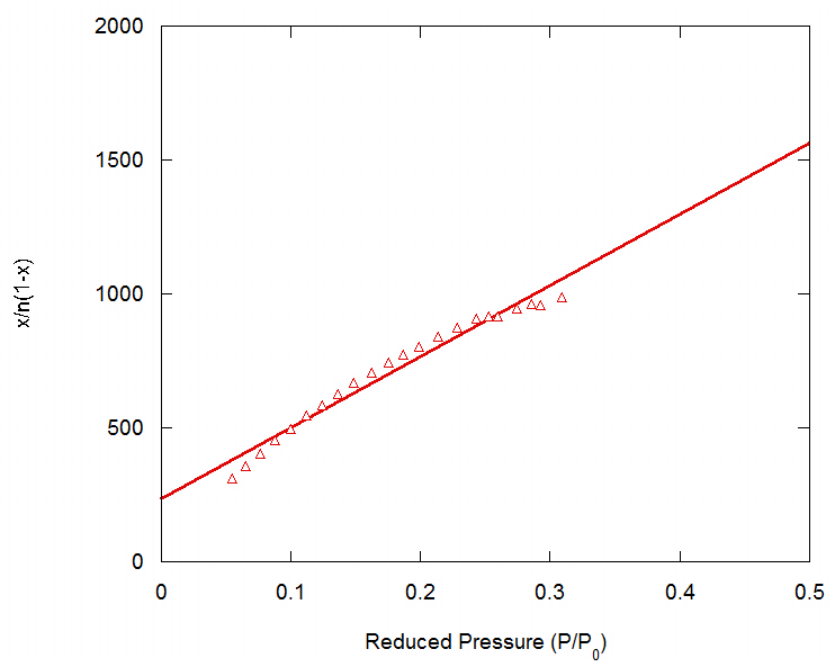


FIGURE 13: Representative BET Plot for Nitrogen on SBA-15 (70.39 K)

Adsorbate	n_m	σ (\AA^2)	Orientation	$A_{\text{monolayer}}$ (m^2)	A (m^2/g)
Methane	2.79E-05	15.4		2.58	25.8
		16.4	Standard	2.75	27.5
		17.3		2.90	29.0
		15.35	2H down	2.57	25.7
		16.261	3H down	2.73	27.2
Ethane	2.17E-05	20.5		2.68	26.8
		19.317	3H down	2.52	25.3
		24.009	4H down	3.14	31.4
Nitrogen	3.46E-04	13.5		28.10	187.35
		14.785	on SBA	30.78	205.18
		16.2	Standard	33.72	224.82

TABLE 2: Table of BET Surface Area Data^{4,16,17}

4.3. Two-Dimensional Compressibility

Using equation [14] above, the two-dimensional compressibility was calculated for each isotherm. Figures 14 and 16 are representative of plots of two-dimensional compressibility versus chemical potential for methane and ethane, respectively. From these, it is difficult to determine whether the peaks observed are truly two separate peaks or just one poorly-resolved peak.

Figures 15 and 16 are plots of two-dimensional compressibility for the data sets of methane and ethane, respectively. In both, the relationship between chemical potential and temperature given in Equation [15] is apparent. Furthermore, both plots reflect the temperature-dependence of the completion of the adsorbed layer being studied. For methane, the reduced pressure at which the second layer is completed is inversely proportional to temperature. In Figure 16, the maximum in two-dimensional compressibility occurs at a lower chemical potential for those isotherms performed at higher temperatures. Considering Equation [14] in which the two-

dimensional compressibility is directly proportional with the derivative of the adsorption isotherm, this relationship becomes apparent.

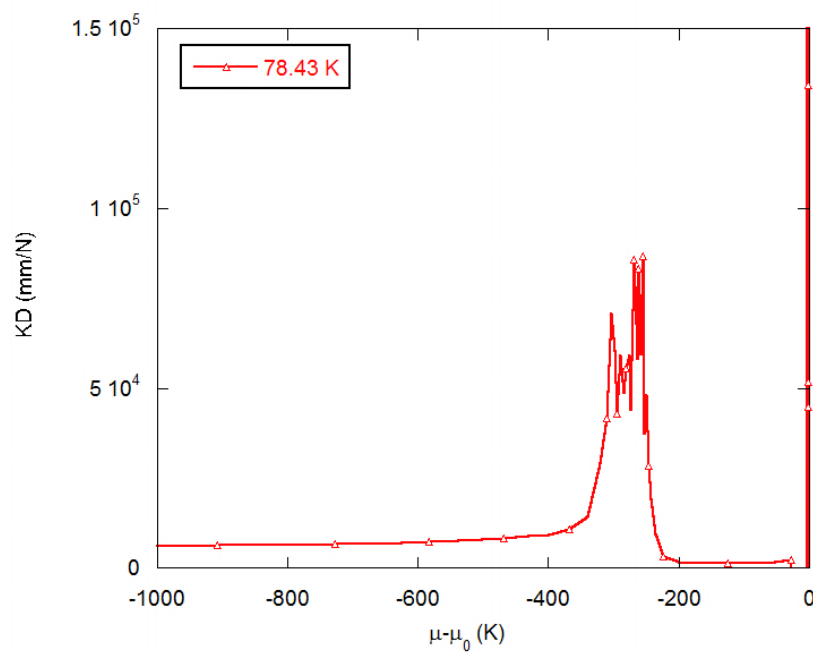


FIGURE 14: Representative Plot of K_{2D} v. $\mu - \mu_0$ for Methane on SBA-15 (78.43 K)

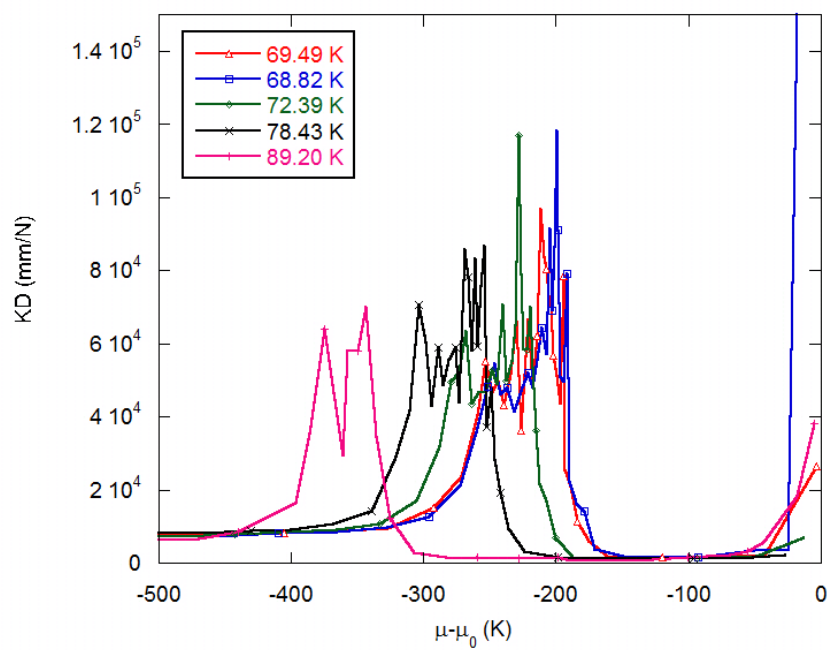


FIGURE 15: K_{2D} v. $\mu - \mu_0$ for Methane on SBA-15

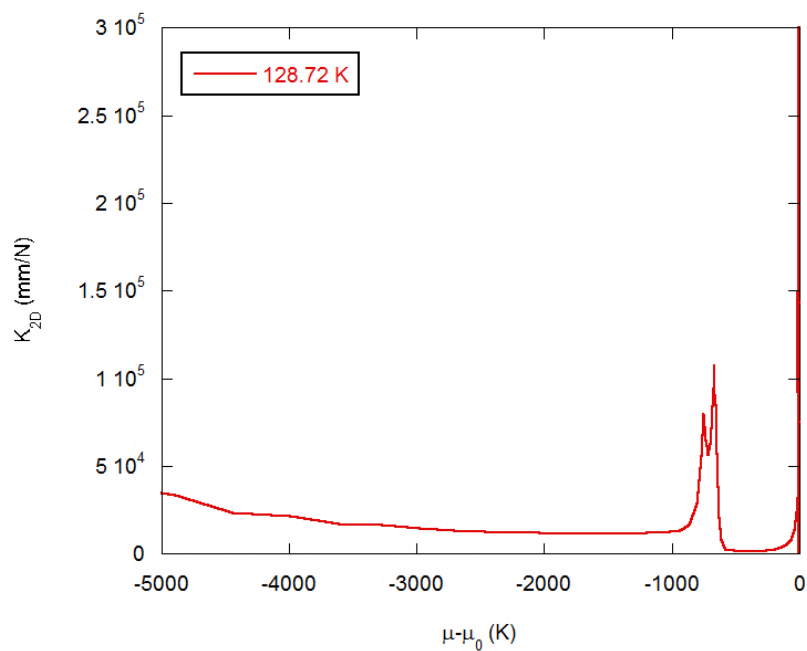


FIGURE 16: Representative Plot of K_{2D} v. $\mu - \mu_0$ for Ethane on SBA-15 (114.15 K)

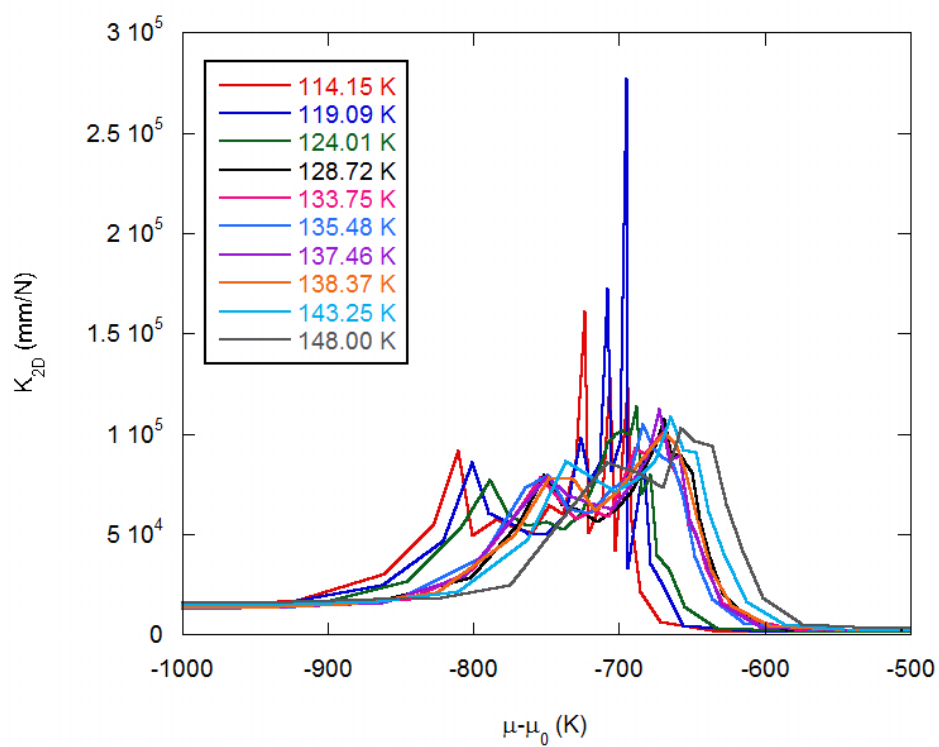


FIGURE 17: K_{2D} v. $\mu - \mu_0$ for Ethane on SBA-15

4.4. Phase Transition

Although plotting the FWHM of the two-dimensional compressibility peak for an adsorption step may prove useful in determining the phase transition, the data in Figures 14-17 make this analysis more difficult for this system. If the peaks are, in fact, two separate local maxima in two-dimensional compressibility potentially corresponding to the filling of the micropores and the mesopores in SBA-15, Figures 15 and 16 demonstrate no marked change in the slope of the linear regression of this FWHM over the temperature range of methane studied. Since a phase transition is marked by a dramatic change in the slope of the linear regression such that two distinct data sets become apparent, it does not appear that methane undergoes a phase transition within this temperature range. Similarly, for the FWHM of the two-dimensional compressibility of ethane plotted with respect to temperature in Figures 20-21, no phase change is apparent.

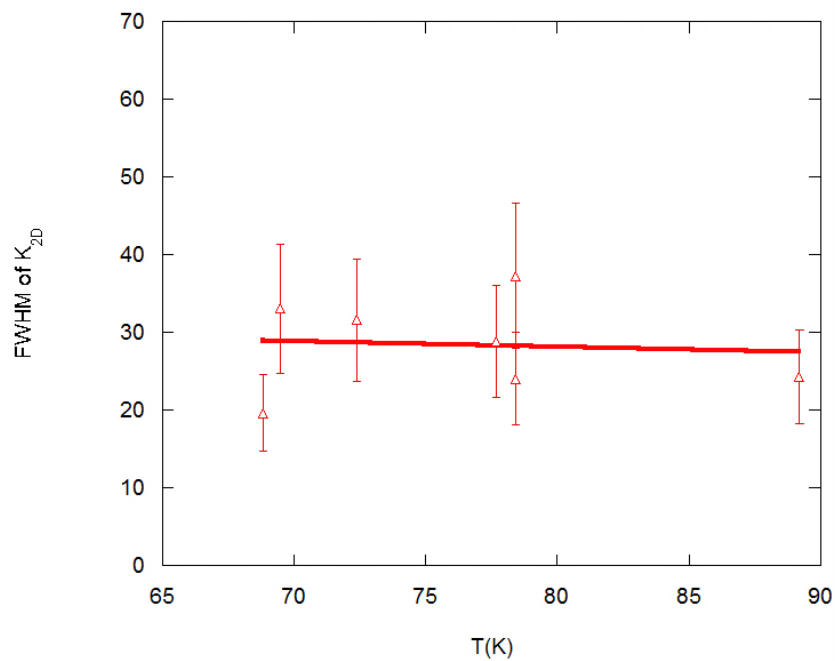


FIGURE 18: Plot of FWHM of K_{2D} versus Temperature for Methane, First Step

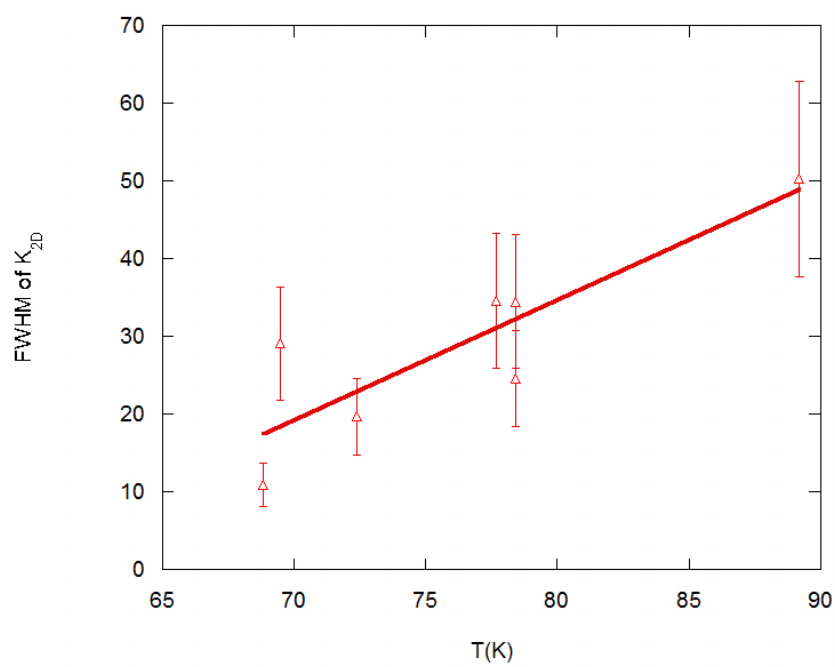


FIGURE 19: Table of FWHM of K_{2D} versus Temperature for Methane, Second Step

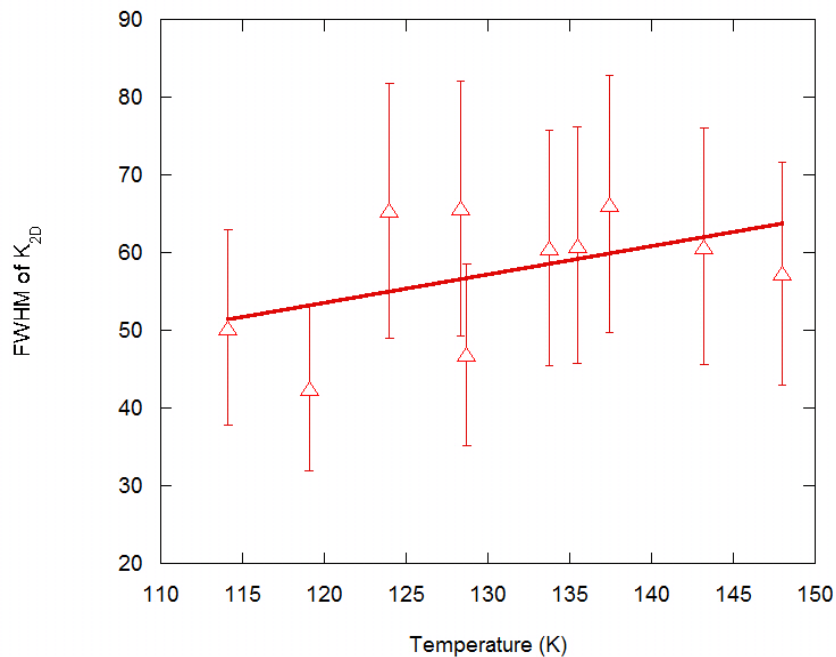


FIGURE 20: Table of FWHM of K_{2D} versus Temperature for Ethane, First Step

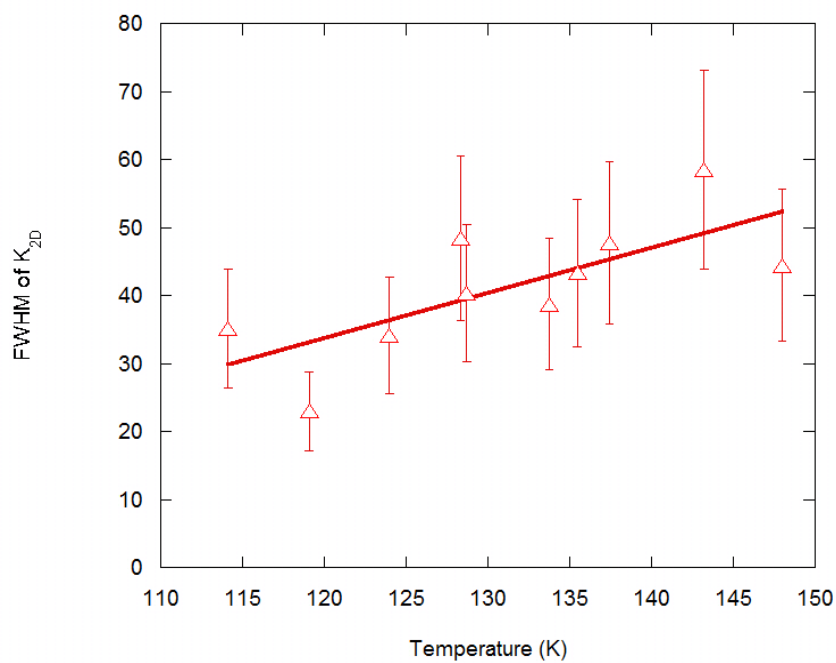


FIGURE 21: Table of FWHM of K_{2D} versus Temperature for Ethane, Second Step

4.5. Dubinin-Astakhov Pore Size Distribution

Using Equations [16-22] and the adsorption isotherm data, the Dubinin-Astakhov pore size distributions of methane and ethane on SBA-15 found in Figures 22 and 24 were created. Based on Figure 22, the pore radius of SBA-15 was found to be between 7.5 nm and 8.0 nm. Since the pore size (diameter) of SBA-15 can be tuned between 5 nm and 15 nm by the conditions of synthesis, this result seems quite reasonable. Furthermore, the pore size distribution is relatively narrow and consistent across a small range of temperatures. As Figure 23 suggests, however, the data reflects a trend in the calculated pore radius with respect to temperature greater than the error.

For the Dubinin-Astakhov pore size distribution of ethane on SBA (Figure 24), the calculated pore radius was approximately 4.45 nm. This is within the range of pore radius values expected for SBA-15. Furthermore, this set of data produced a very narrow peak with a variation in pore radius only visible at the small scale used in Figure 24. At larger scales, the distinction among the different temperatures disappeared, and the different data sets were difficult to discern. As Figure 25 demonstrates, the pore size did not show a marked relationship with temperature over the 30 K temperature range studied.

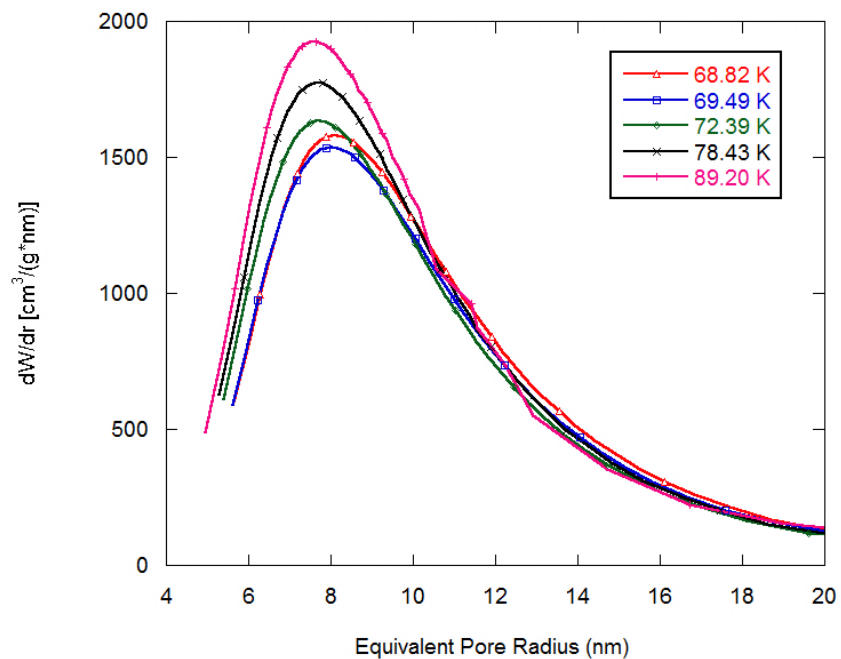


FIGURE 22: Plot of dW/dr versus Equivalent Pore Radius for Methane

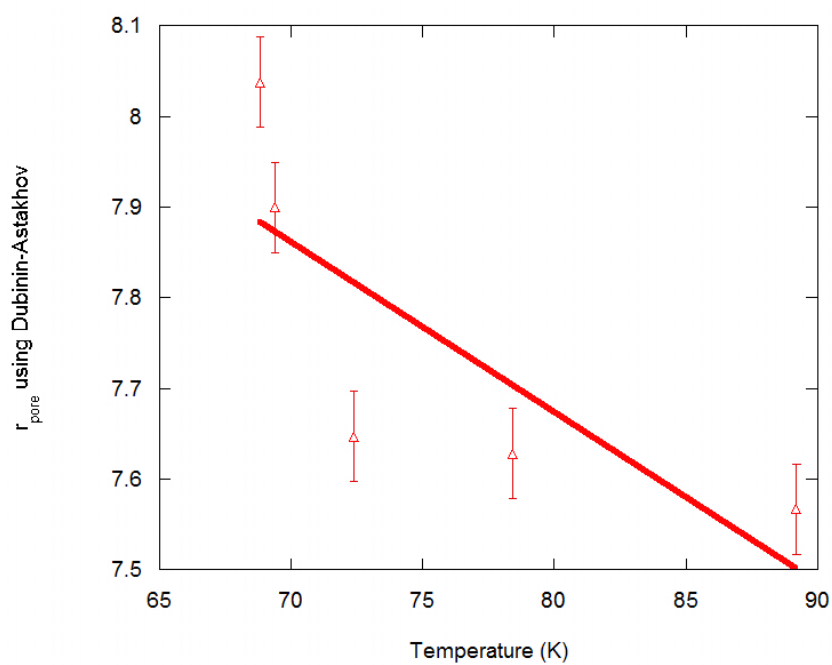


FIGURE 23: Plot of Equivalent Pore Radius versus Temperature for Methane

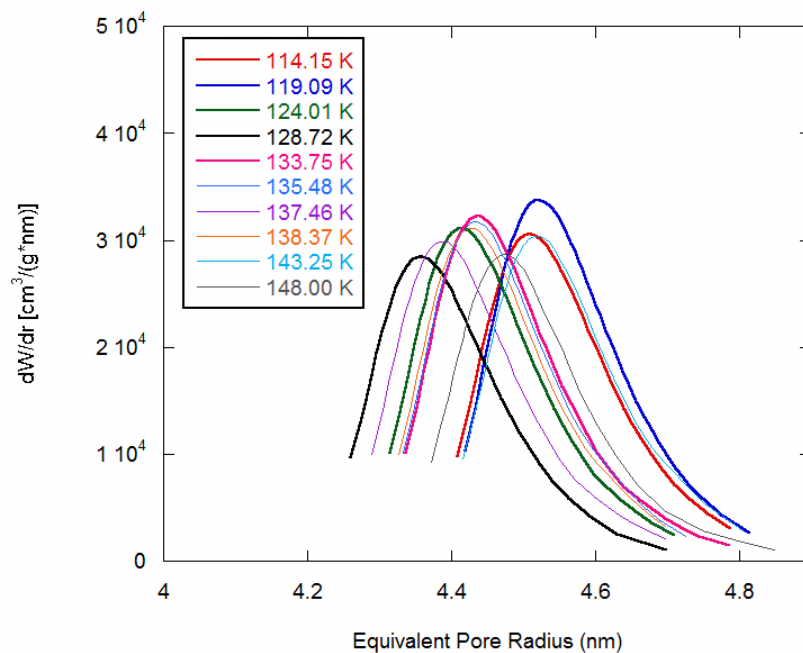


FIGURE 24: Plot of dW/dr versus Equivalent Pore Radius for Ethane

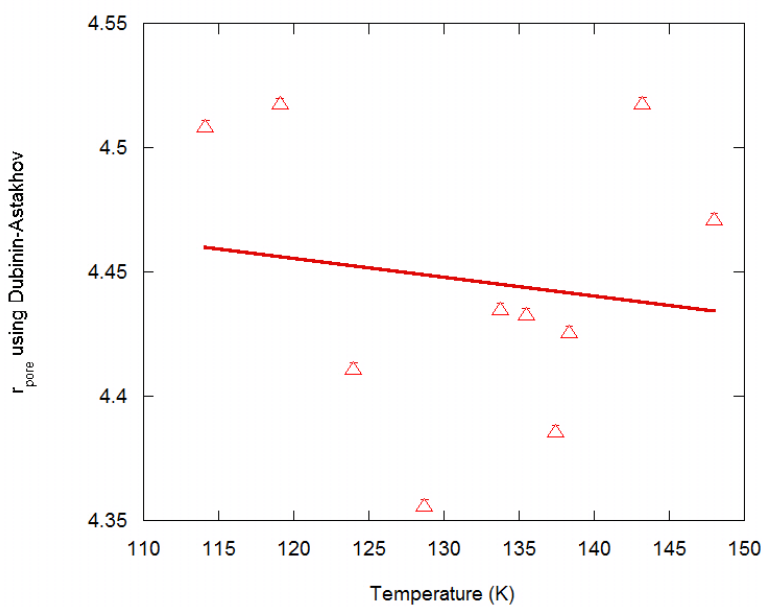


FIGURE 24: Plot of Equivalent Pore Radius versus Temperature for Ethane

4.6. Kelvin Equation Pore Size Distribution

Using Equations [9,23-24], a pore size distribution based on the Kelvin equation was created. Figure 25 is the Kelvin equation pore size distribution for methane, which reflects the same peaks in the data found in previous plots involving the two-dimensional compressibility. The range of pore radius values, 2.5 nm to approximately 7.0 nm is within that expected for SBA-15. This data suggests the temperature-dependence of pore radius calculated using the Kelvin equation, but further analysis of this data was omitted.

For the adsorption of ethane onto SBA-15, the average pore radius was found to be within the range of 3.2 nm to 3.9 nm based on Figure 26. These values lie within the range expected for SBA-15. Further analysis of the data would be necessary to assess the validity of any claims regarding the temperature-dependence of the pore radius of SBA-15 calculated using the Kelvin equation.

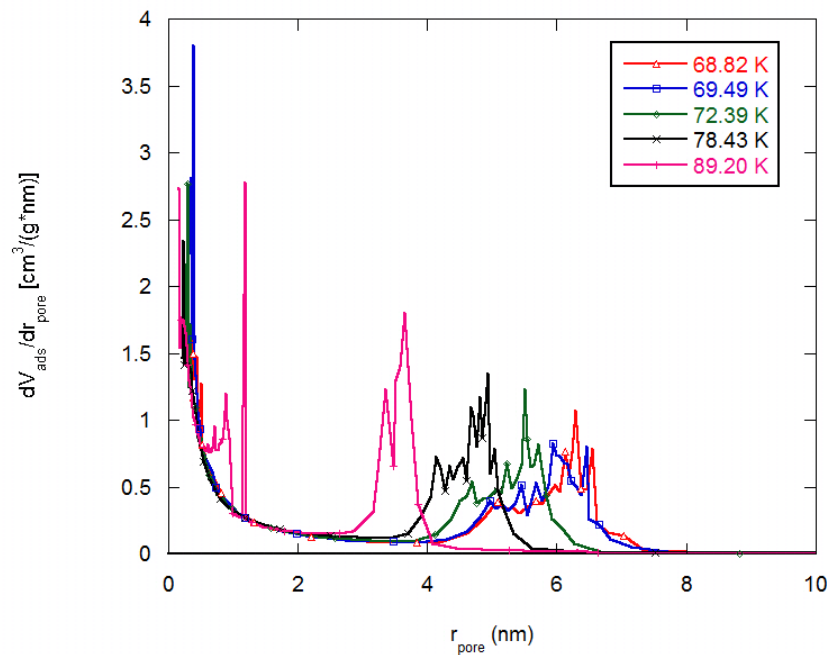


FIGURE 25: Plot of Pore Size Data for Methane on SBA-15 (69.49 K – 89.21 K)

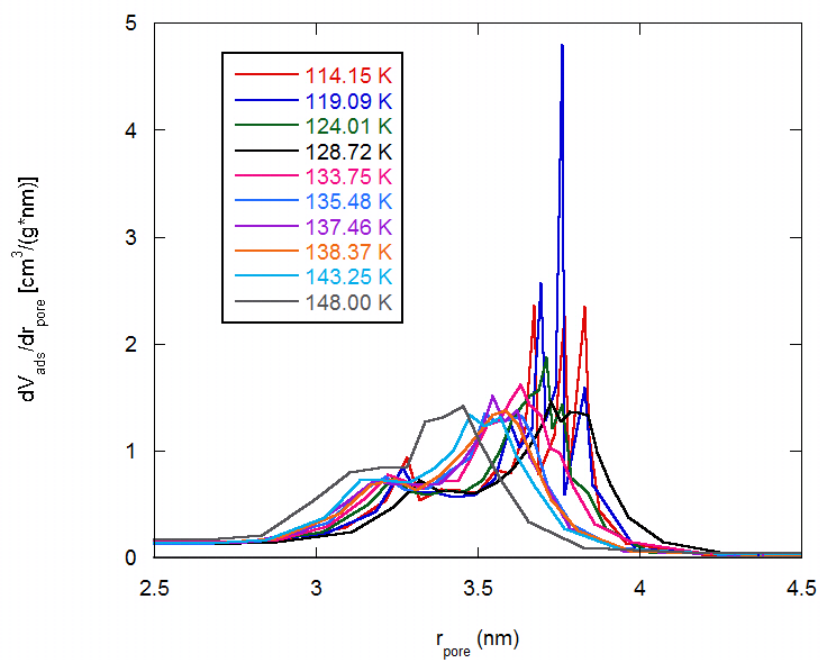


FIGURE 26: Plot of Pore Size Data for Ethane on SBA-15 (114.19 K – 148.00 K)

4.7. Clausius-Clapeyron

The Clausius-Clapeyron equation can be used to calculate several thermodynamic quantities from a plot of final pressure for the completion of a given layer of adsorbed gas versus inverse temperature. In all of the trials completed, the monolayer was completed at a pressure too low for inclusion in the calculations. Figures 8 and 10 show two nearly-overlapping peaks in the first derivative plot. This suggests that the completion of the second layer of adsorbed gas molecules occurs in two overlapping steps, presumably completion of the second layer in the mesopores and micropores separately.

In Figures 27 and 28, the Clausius-Clapeyron plots for methane and ethane, respectively, on SBA-15 are displayed. The line corresponding to the lowest pressures represents the line of best fit for the completion of the second layer of adsorbed gas molecules in the micropores. The second line corresponds to the completion of this layer in the micropores while the data at highest values of $\log(p)$ reflects the bulk. The calculated values found in Tables 3 and 4 reflect the differences in the adsorbate-adsorbent interactions between the methane and ethane on SBA-15 as well as the effect of pore size on adsorption for the two gases. For methane, the differences in energy between adsorption in the mesopores and micropores were generally quite small, which suggests that methane adsorption occurs similarly in both. However, the thermodynamic differences for ethane adsorption in the mesopores and micropores were approximately 100 J/mol for both the enthalpy and heat of adsorption. This suggests that ethane adsorbs differently based on pore size.

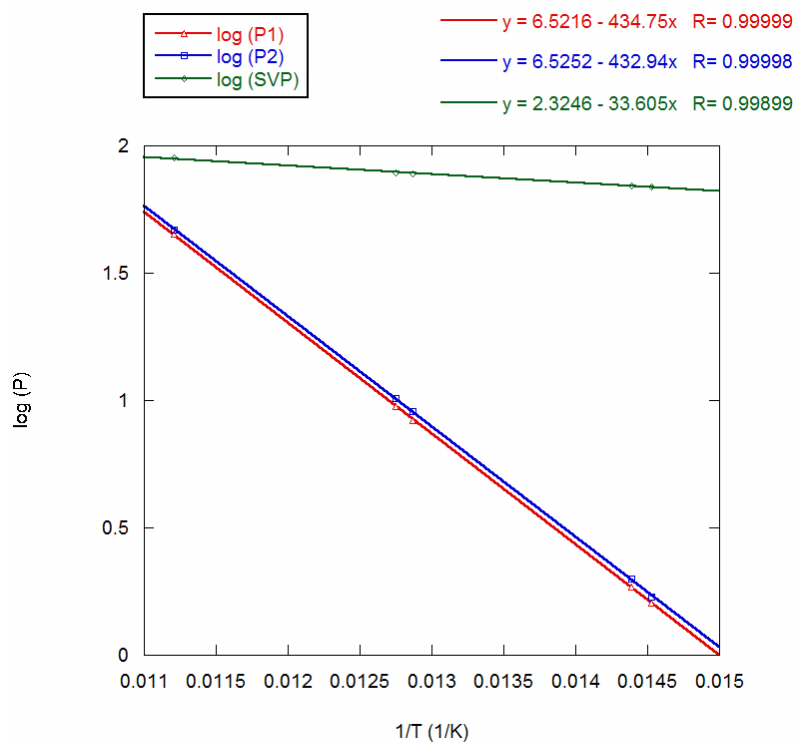


FIGURE 27: Clausius-Clapeyron Plot for Methane on SBA-15

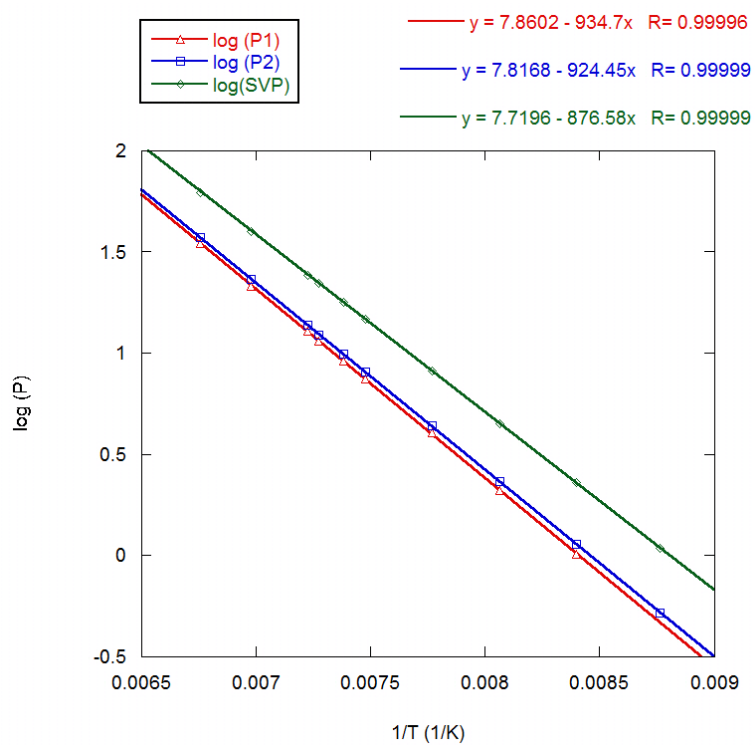


FIGURE 28: Clausius-Clapeyron Plot for Ethane on SBA-15

N	A ⁿ	B ⁿ	ΔH_{trs} (J/mol)	ΔS_{trs} (J/mol)	ΔQ_{trs} (J/mol)
N=2, Mesopore	434.8	6.522	-3335	-34.89	3615
N=2, Micropore	432.9	6.525	-3320	-34.93	3600
N= ∞	33.61	2.325	---	---	279.4

TABLE 3: Methane on SBA-15 Thermodynamic Data

Ethane	A ⁿ	B ⁿ	ΔH_{trs} (J/mol)	ΔS_{trs} (J/mol)	ΔQ_{trs} (J/mol)
N=2, Mesopore	934.7	7.860	-483.2	-1.169	7771
N=2, Micropore	924.4	7.817	-398.0	-0.8082	7686
N= ∞	876.6	7.720	---	---	7288

TABLE 4: Ethane on SBA-15 Thermodynamic Data

5. Conclusion

From a series of adsorption isotherms of methane, ethane, and nitrogen on SBA-15, various quantities were calculated in order to characterize the surface of SBA-15 and the adsorbate-adsorbent interactions. Based on the BET plots and subsequent surface area calculations, it appears that nitrogen is superior to either methane or ethane for determining the surface area. In order to confirm this assertion, more adsorption isotherms over a larger range of temperatures would be necessary. Using each of these samples on the same sample of SBA-15 rather than just samples from the same batch would also improve the validity of these results. The point-B method could have also been used as an alternate means of calculating surface area.

Based on the plots of two-dimensional compressibility, it is difficult to characterize the local maxima in the derivative of the adsorption isotherm as being two distinct layering steps or one step completed over a larger range of relative pressures. The plots of FWHM do not support an assertion that a phase transition for methane on SBA occurs over the range of 68.82K to 89.21K. Similarly, the data do not suggest a phase transition of ethane on SBA over the temperature range of 114.15K to 148.00K. In order to make any further conclusions regarding this data, a smoother adsorption isotherm would be necessary. This goal could be accomplished by applying a smoothing fit to the experimental data or completing isotherms using a smaller step size. If a larger temperature range were used, the phase transitions may become apparent.

Using the Dubinin-Astakhov model produced good results for the pore size distribution and was much easier than using the Kelvin equation for the systems under study. While the parameters necessary to solve the Kelvin equation were sometimes

difficult to locate or required an approximation, those necessary for calculating molar polarizability were located quickly. In both cases, the pore radii determined for SBA-15 were within the range of expected values. However, the different pore size values for methane and ethane using both Dubinin-Astakhov and Kelvin equations suggest that further refinements should be made. In order to optimize the Dubinin-Astakhov results, the Astakhov coefficient, N , could be varied over a larger range than 1.0000 to 3.000. Since the Kelvin equation has been found to underestimate pore size by about 25% for many mesoporous systems,⁴ it is unlikely that any further refinements would eliminate the uncertainty in this result short of using non-localized density functional theory. In the interest of assessing these values, other methods of determining pore size such as adsorption-desorption isotherms, small-angle x-ray scattering, or neutron scattering.

Based on the Clausius-Clapeyron plots, the difference in thermodynamics of the adsorption of methane and ethane became apparent. Completing adsorption isotherms over larger temperature ranges such that a more significant trend could have been located would have been useful.

Overall, these sets of data suggest that both Dubinin-Astakhov and Kelvin equations return similar results for calculating the surface area of SBA-15. This effectiveness may be due to the presence of micropores for which Dubinin-Astakhov theory was developed as well as mesopores for which the Kelvin equation was developed. Although Dubinin-Astakhov theory has traditionally been used to assess the pore size of microporous carbon surfaces, the results suggest the applicability of its extension to a primarily mesoporous silica material.

References

- ¹ Himeno, Shuji; Urano, K. *Journal of Environmental Engineering Science* **2006** 3, 301.
- ² Hsieh, Chieng-To; Teng, H. *Carbon* **2000** 38, 863-869.
- ³ Zhou, Li; Liu, J.; Su, W.; Sun, Y.; Zhou, Y. *Energy Fuels* **2010** 24, 3789.
- ⁴ Lowell, S.; Shields, J. E.; Thomas, M. A.; Thommes, M. *Characterization of Porous Solids and Powders: Surface Area, Pore Size and Density*; Springer, 2006.
- ⁵ Adamson, A.W., *Physical Chemistry of Surfaces*, 6th ed., Wiley: New York, 1997, p. 599.
- ⁶ Dubinin, M. M. *Carbon* **1985** 4, 373.
- Dubinin, M. M.; Kadlec, O. *Carbon* **1987** 25 (3), 321.
- Dubinin, M.M. *Carbon* **1987** 25 (5), 593.
- ⁷ Gauden, P. A.; Terzyk, A. P.; Rychlicki, G.; Kowalczyk, P.; Cwiertnia, M. S.; Garbacz, J. K. *Journal of Colloid and Interface Science* **2004** 273, 39-63.
- ⁸ Wood, G.O. *Carbon* **2001** 39, 343-356.
- ⁹ Zhao, D.Y.; Feng, J. L.; Huo, Q. S.; Melosh, N.; Frederickson, G. H.; Chmelka, B. F.; Stucky, G. D. *Science* **1998** 279, 548-552.
- ¹⁰ Thielemann, Jörg; Girgsdies, F.; Schlögl, R.; Hess, C. *Beilstein Journal of Nanotechnology* **2011** 2, 110-118.
- ¹¹ Zholobenko, Vladimir L.; Khodakov, A. Y.; Impéro-Clerc, M.; Durand, D.; Grillo, I. *Advances in Colloid and Interface Science* **2008** 142, 67-74.
- ¹² Kokunešoski, M.; Gulicovski, J.; Matović, B.; Logar, M.; Milonjić, S. K.; Babić, B. *Materials Chemistry and Physics* **2010** 124, 1248-1252.
- ¹³ NIST WebBook.
- ¹⁴ *Handbook of Chemistry & Physics, 92nd Edition*; CRC Press, 2011-2012. Online version.

-
- ¹⁵ Yaws, Carl L; Narasimhan, P.; K.; Gabbula, C. *Yaws' Handbook of Antoine Coefficients for Vapor Pressure (2nd Electronic Edition)*; Knovel, 2009. Online version.
- ¹⁶ McClellan, A. L.; Harnsberger, H. F. *Journal of Colloid and Interface Science* **1967** 23, 577-599.
- ¹⁷ Webster, Charles Edwin; Drago, R. S.; Zerner, M. C. *Journal of the American Chemical Society* **1998** 120, 5509-5516.
- ¹⁸ Frietag, Andrea; Larese, J.Z. *Physical Review B* **2000** 62 (12), 8360-8365.
- ¹⁹ Larher, H.; Angerand, F. *Europhysics Letters* **1988** 7, 447.
- ²⁰ "TriStar 3000 User Manual, Appendix C," Micromeritics.